Highly explosive eruption of the monogenetic 8.6ka BP La Vache et Lassolas scoria cone complex (Chaîne des Puys, France)

Simone Jordan, Jean-Luc Le Pennec, Lucia Gurioli, Olivier Roche, Pierre Boivin

Highly explosive eruption of the monogenetic 8.6 ka BP La Vache et Lassolas scoria cone complex (Chaîne des Puys, France)

S.C. Jordan*, J.-L. Le Pennec, L. Gurioli, O. Roche, P. Boivin

Laboratoire Magmas et Volcans, Université Blaise Pascal-CNRS-IRD, OPGC, 5 rue Kessler, 63080 Clermont-Ferrand, France

The eruption of the trachy-basaltic La Vache and Lassolas cone complex was the youngest eruption (ca. 8.6 ka BP) and one of the most violent in the Chaîne des Puys, France. Here we present field data and results of grain size, componentry and clast density measurements of different layers of the widespread tephra deposit that is associated with this cone-forming eruption. Our data indicates five main eruption phases comprising a vent-opening phase, a second sustained highly explosive phase, a third and fourth violent Strombolian phase and a fifth dominantly effusive phase. The layer formed by the opening phase is rich in lithic material, which was previously considered to be the result of phreatomagmatic activity. The data presented here on the componentry and textures of the pyroclastic material contradict this hypothesis. We propose instead that the material of the basal layer results from fragmentation caused by the explosion of a first arriving gas-dominated phase. The variations in eruption intensity during the main eruption phases are interpreted here to be the result of gas segregation within the plumbing system and fluxes in the magma ascent rate during the eruption. Significant amount of gas segregation is indicated by the deposition of both gas-poor and gas-rich material and by the presence of plate tephra. This is also supported by the simultaneous ejection of tephra and lava from both cones during most of the explosive activity. We suggest that gas segregation occurred within shallow intrusions and that fresh ascending material in the main conduit mixed with degassed material that flow back into the conduit from the intrusion before fragmentation. The interaction of the ascending magma and the opening of intrusions may have controlled the evolution and explosivity of the eruption. The high explosivity at the beginning of the eruption and the wide dispersal area, demonstrate that scoria cone eruptions in monogenetic fields can impose a major threat to the population and infrastructures nearby as these events may occur with little warning, and therefore research on this kind of eruptions is of a major importance to better understand the processes driving these events.

1. Introduction

Scoria cones are generally considered to be formed by small volume, monogenetic eruptions that are predominantly Strombolian in style (McGetchin et al., 1974). However, recent research has shown that purely Hawaiian and sub-Plinian style eruptions can also form scoria cones (Riedel et al., 2003; Valentine et al., 2005; Pioli et al., 2008; Guilbaud et al., 2009; Kawabata et al., 2015). In addition, scoria cone forming eruptions can simultaneously produce long lava flows and widespread tephra deposits that have been described as the product of violent Strombolian activity (Pioli et al., 2008, 2009; Di Traglia et al., 2009; Cimarelli et al., 2010; Németh, 2010; Kiyosugi et al., 2014). The term violent Strombolian eruption has been used for eruption events that produced eruption columns of <1010 km height and therefore lower than sub-Plinian ones, while Strombolian type eruptions eject pyroclastic material during discrete intermittent explosions, only up to a few hundreds of metres (Riedel et al., 2003; Valentine et al., 2005; Pioli et al., 2008; Németh, 2010). Historically observed scoria cone eruptions lasted from days to years, with rapid growth within the first few days and had time-averaged mass eruption rates (MERs) in the order of 10^{2} to 10^{5} kg/s (Wood, 1980; Riedel et al., 2003; Pioli et al., 2009; Rowland et al., 2009).

In the last decade growing research on scoria cone-forming eruptions showed that this type of eruptions can produce plume-derived tephra fall deposits extending over tens of kilometres from the vent (Valentine et al., 2005; Pioli et al., 2008; Rowland et al., 2009; Johnson et al., 2014) and that these eruptions may pose a serious hazard to populations living within or in the vicinity of monogenetic volcanic fields (Guilbaud et al., 2009). While the traditional model by McGetchin et al. (1974) suggested formation of the cone by accumulation of ballistic material, studies by Riedel et al. (2003), Valentine et al. (2005) and Mannen and Ito (2007) indicate that scoria cones may form rapidly by fallout of coarse material from the lower part of the eruption column associated with violent Strombolian or sub-Plinian eruptions.

* Corresponding author.
E-mail address: S.Jordan@opgc.univ-bpclermont.fr (S.C. Jordan).

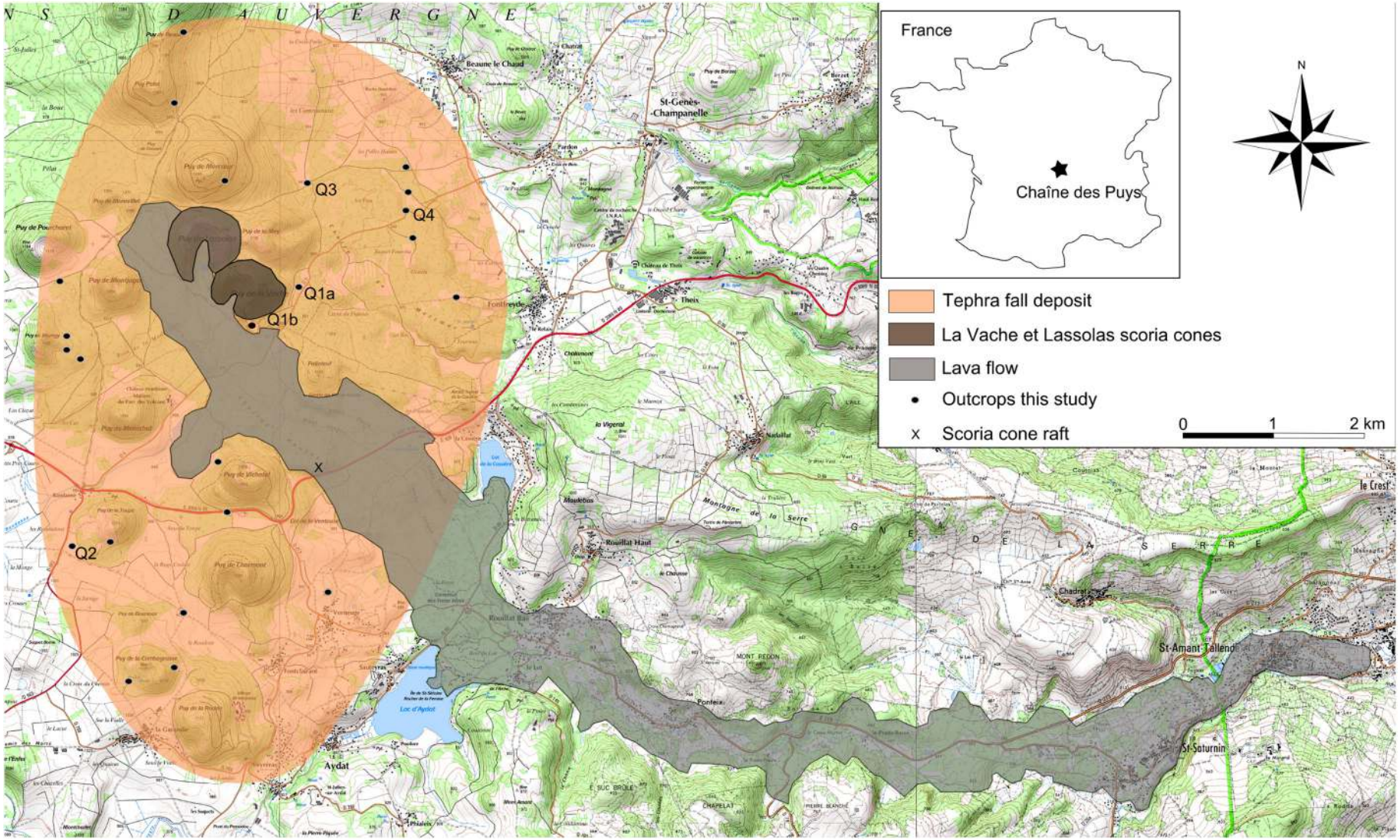

Fig. 1. Map of the La Vache and Lassolas eruption products showing the dispersal area of the tephra deposit, the two scoria cones and the extension of the associated lava flow.

The study presented here on the eruption of the La Vache and Lassolas scoria cones is an example for a complex scoria cone forming eruption. The twin scoria cones are located in the Chaîne des Puys volcanic field, France, and erupted trachy-basaltic magma with phases of high intensity, explosive activity, violent Strombolian style activity and quiet lava effusion (Fig. 1). The relatively young age of ca. 8.6 ka BP derived from C ^{14} dating (Miallier 2015, personal communication) and the fresh pyroclastic material of this eruption makes the La Vache and Lassolas cones an excellent natural laboratory to investigate the processes that led to this highly explosive eruption. Only little work in the broader context of the Chaîne des Puys has been done on this volcanic complex by Baudry and Camus (1969) and Camus (1975). In this study, detailed stratigraphic analysis comprising grain size, componentry and clast density gives insights into the dynamics of this violent eruption that produced two large twin scoria cones, a long lava flow and a widespread tephra deposit.

2. Geological setting

The monogenetic Chaîne des Puys volcanic field comprises 80 volcanic centres, including basaltic scoria cones, maars and trachytic domes (Miallier et al., 2004; Jannot et al., 2005; Boivin et al., 2009). The uniqueness of the geological setting of this volcanic field along the Limagne graben fault gave the initiation to make this area a candidate for the UNESCO World Heritage site (Boivin and Thouret, 2013; Delcamp et al., 2014). Volcanic activity is occurring in the Chaîne des Puys area since 5 Ma years. The formation of the recent main volcanic chain started around 70 ka BP and ended with the trachy-basaltic eruption of La Vache and Lassolas (Boivin et al., 2009). The emplacement of the volcanic centres occurred along N/NE to S/SW oriented faults (Boivin et al., 2009).

The two scoria cones of La Vache and Lassolas are located directly against to the older La Mey and Merceur scoria cones (Fig. 1), indicating an earlier volcanic activity in this area. La Vache and Lassolas are horse shoe-shaped, with an opening of the craters towards the south. La Vache is 187 m high with a base diameter of 799 m and a diameter at the crater rim of 415 m, while Lassolas is 200 m high with a base diameter of 894 m and a diameter at the crater rim of 475 m. The Lidar image of La Vache and Lassolas (Fig. 2) suggests rifting of the western flank of Lassolas towards the southwest, which may be the result of magma intruding at the base of the cone. Both cones fed a 22 km-long lava flow (Fig. 1) that dammed a valley, forming the two recent lakes, Lac d'Aydat and Lac de la Cassière. The lava flow transported parts of the scoria cones as rafts downstream. One of these rafts is exposed outside the main lava channel ca. 2 km downstream of the scoria cones (Fig. 1). In addition, the eruption produced a widespread tephra fall deposit that is investigated in detail in this study.

3. Analytical methods

3.1. Thickness measurements and sampling

The thickness of the tephra deposit was measured at 23 outcrops during detailed field mapping. The measurements were plotted on a topographic map (Fig. 1), and the isopach contours for 800 cm, 100 cm, 75 cm, 45 cm and 25 cm were constructed for the total tephra deposit. Isopachs below the 25 cm isopach line could not be drawn confidently. Five key sections of the tephra fall deposit, shown on the geological map (Fig. 1), were sampled in detail, with 19 samples for section Q1a, 5 samples for section Q1b, 10 samples for section Q3, 6 samples for section Q2 and one sample for the off-axis section Q4.

3.2. Grain size analysis and componentry

The samples were dried in the oven at 90 C and sieved at $\frac{1}{2}\phi$ intervals in the range of -3ϕ to 4ϕ. Sieving was carried out by hand and for not longer then three minutes to avoid breaking and abrasion of the very vesicular and fragile clasts even for the coarse ash portion of the deposits to avoid breakage of elongated features. The majority of the examined clasts is intact, however, a small amount of clasts (< 10 vol.%) shows signs of breakage after fragmentation. Afterwards each size fraction was recovered from the sieves and weighed to determine the weight percent of each size fraction and to calculate sedimentary parameters such as Median grain size and sorting using Inman (1952) definitions.

In addition, the componentry was determined for each grain size fraction between -5.0ϕ and 0.5ϕ, where a binocular microscope was used for the identification of grains smaller than -1.0ϕ. The samples did not need any special cleaning because the tephra is essentially fresh and not ash-coated. For homogeneity reasons each sample was turned in its container several times before a small amount of grains was extracted for the analysis from the middle of the sample. Eychenne et al. (2013) have demonstrated that it is necessary to identify at least 250 clasts to gain stable componentry proportions within 2– 3% uncertainty, therefore a statistical relevant number of 500 grains or the

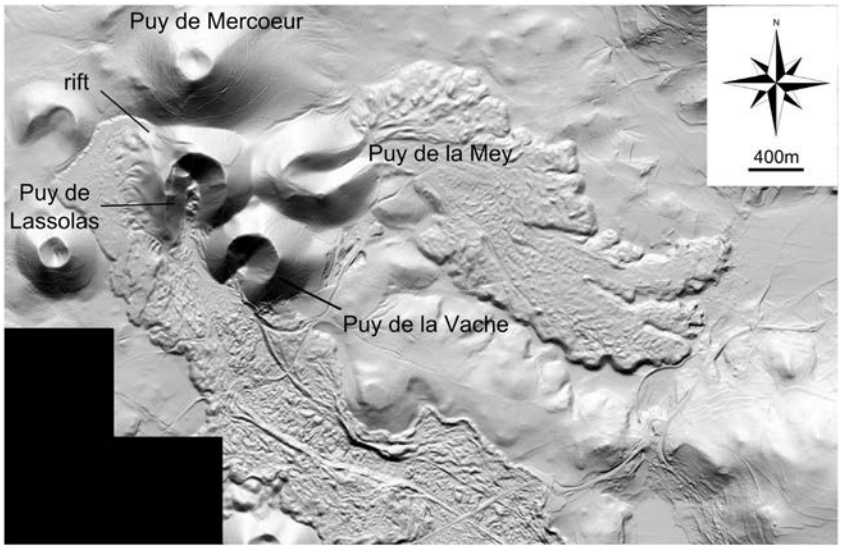

Fig. 2. Lidar image (source: CRAIG-APEI-SINTEGRA 2013) of the two horse shoe shaped scoria cones Puy de la Vache and Puy de Lassolas, showing the associated lava flow and the rifted southwestern flank of Puy de Lassolas.

total size fraction was counted for each size fraction and the vol.% provided. The 500 grains were counted in steps of 10 grains to control the stability of the results and to check for any bias introduced by the analyst.

Five types of clasts were determined (Fig. 3): 1) spiny scoria, 2) rounded scoria, 3) platy juvenile clasts, 4) magmatic free crystals and 5) lithic clasts (polycrystalline clasts and free crystals from the granitic basement).

Type 1 clasts are dark, spiny scoria that vary in shape from subrounded to angular and are predominantly glassy (Fig. 3a).

Type 2 clasts consist of rounded to subrounded scoria (Fig. 3b). The majority of these clasts have grey, smooth surfaces, but their interior can be both dense or vesicular. Some clasts have a single large phenocryst as a core.

Type 3 are juvenile clasts that are flat with a platy curviplanar shape, with some clasts showing bending and contortion (Fig. 3c). The clasts are typically poorly to non-vesicular, dark in colour and are generally glassy.

Type 4 are free juvenile crystals, including augites (Fig. 3d), olivines and plagioclases, with a general ratio of augites to olivine + plagioclase of 9:1 in all samples. All phenocrysts have an euhedral to subeuhedral shape, however, ca. 80% of the crystals are fractured, where fracturing in the augites occurred predominantly along the long axis.

Type 5 are accidental lithic country rock fragments consisting predominantly of whitish to yellowish granitic fragments from the basement (Fig. 3e). In the coarse grain size fractions (-5 – -1.5ϕ) the granitic fragments occur as polycrystalline grains, while in the smaller grain size fractions (-1 – 0.5ϕ) these lithics occur as single crystals of quartz, feldspar and mica. In addition, these crystals are only slightly altered and not covered by any ash or juvenile material.

3.3. Density

Clast density was determined for three different size fractions when possible, -3ϕ – -3.5ϕ, -3.5ϕ – -4ϕ, and the 100 largest clasts within the range of -4.5ϕ – -5.5ϕ in diameter. The method of Houghton and Wilson (1989) was used, where the weight of each clast is measured once before it is wrapped in a thin sheet of parafilm and second after wrapping and immersing in water. The specific gravity (S.G.) for the clast can be calculated as following:

$$S.G. = \frac{W_c air}{W_c air + W_s water - W_{c+s} water} \quad (1)$$

with W_c being the weight of the clast in air or in water and W_s being the weight of the parafilm sheet. The density is then obtained by dividing the specific gravity by the density of water (1000 kg/m ^{3}). The study of Barker et al. (2012) on the precision of this method showed that the maximal introduced error is 30 kg/m ^{3}.

4. Field relationships, eruption products and their distribution

4.1. Deposits along the main dispersal axis

The most complete section Q2 is disclosed in a recently excavated trench that is located 3.4 km south east of La Vache (Fig. 1). The tephra of the La Vache and Lassolas eruption forms the upper most volcanic layer underneath the topsoil and can be well distinguished from older underlying volcanic deposits (Fig. 4). The first layer (L1) consists of fine lapilli, is 5 – 8 cm thick (Fig. 5), well sorted and contains abundant (20– 30%) whitish–yellowish granitic clasts (Fig. 6). Proximal to the vent L1 is 20 cm thick and contains some granitic blocks (up to 15 cm in diameter). A sharp contact separates L1 from the overlying well sorted lapilli layer (L2) that is 8 cm thick in Q2 and is formed by highly vesicular scoria. In the proximal section, L2 is 175 cm thick, massive and inversely graded from fine lapilli at the base to very coarse lapilli at the top (Fig. 7). L2 is overlain in Q2 by a 2 cm thick, slightly indurated, fine lapilli ash layer (A1) that is missing in the proximal section Q1. The overlying scoria lapilli layer (L3) is 7 cm thick in Q2 and shows subtle lens-bedding in some distal parts. In the proximal area, L3 is 560 cm thick and again inversely graded from coarse lapilli at the base to very coarse lapilli near the top. The uppermost part in the proximal area, however, has a finer medium lapilli grain size and is separated from the lower part of the layer by a train of scattered bombs (Fig. 7). In addition, bombs up to 8 cm in diameter are scattered throughout the layer. In the upper half of the layer, however, they form a difuse stratification with a vertical spacing of the bomb trains of roughly 20 cm

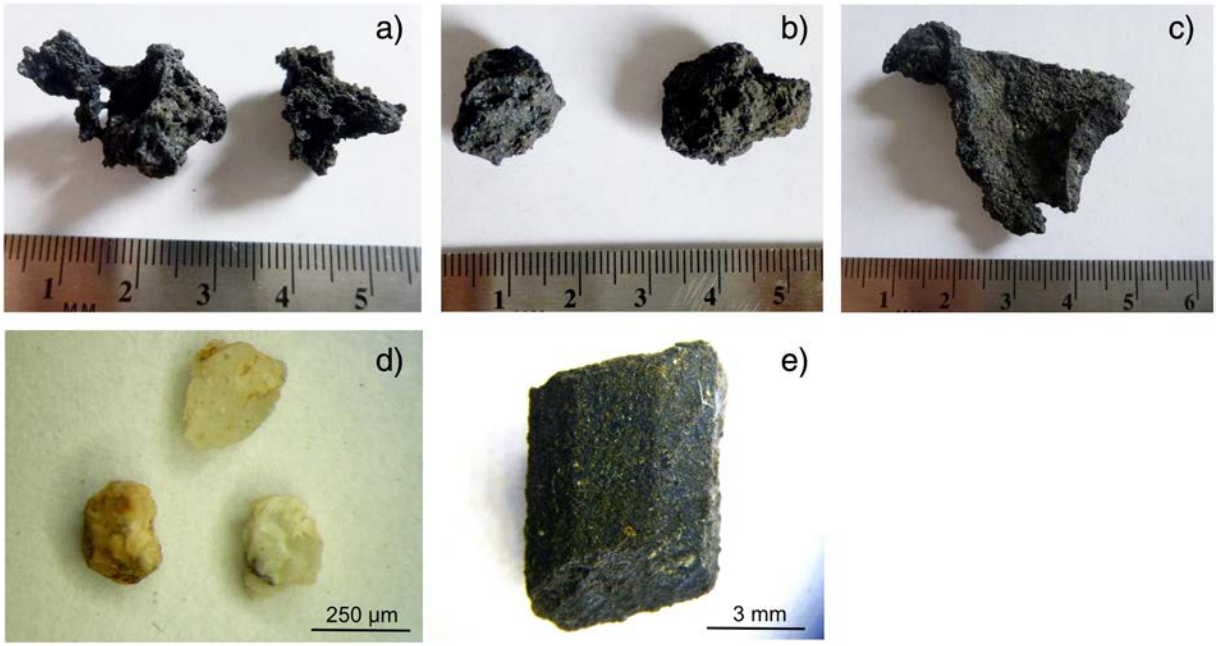

Fig. 3. Images of the five different clast types such as a) vesicular juvenile clasts, b) subrounded juvenile clasts, c) platy juvenile clasts, d) magmatic crystals and e) granitic lithic clasts.

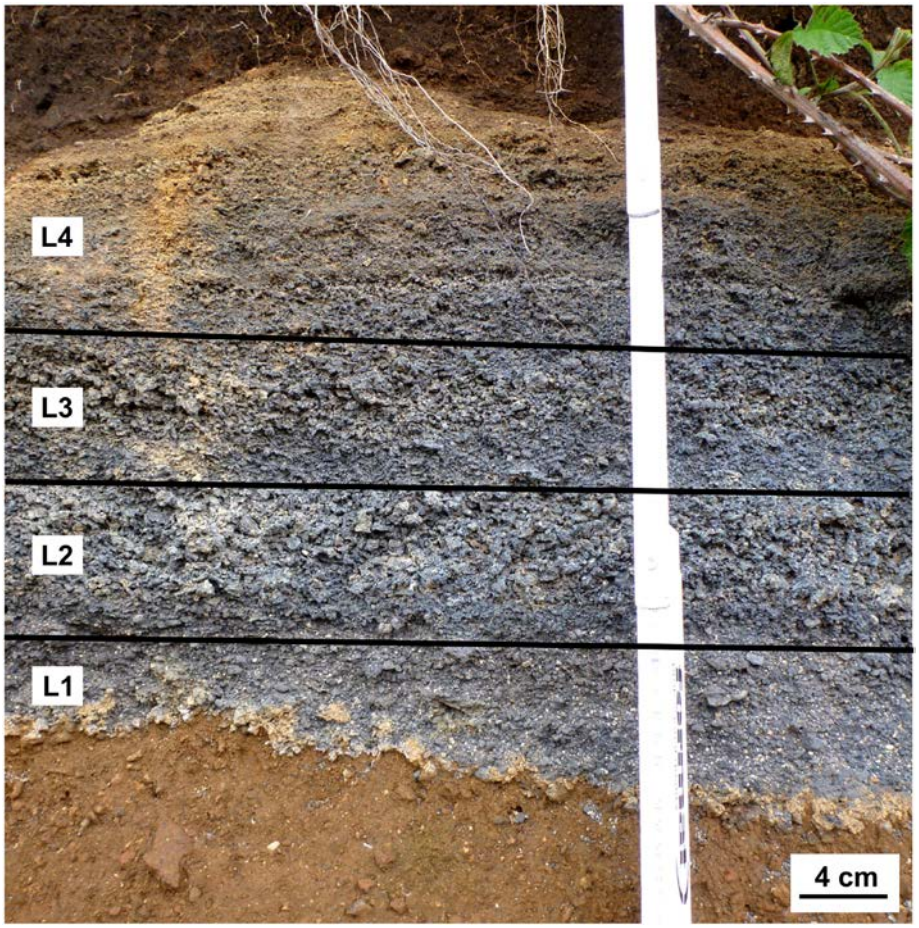

Fig. 4. Complete section of the relative distal La Vache and Lassolas tephra, including underlying older volcanic deposits, lapilli layers 1–4 and the topsoil.

(Fig. 7). The layer (L4) on top of L3 is formed by fine lapilli-sized scoria and is 8 cm thick in Q2. Two 1 cm thick ash layers are present at the top in Q2 that are separated by a 3 cm thick lapilli layer. In the proximal these two ash layers occur 90 cm above the L3/L4 boundary and are separated by a 10 cm thick lapilli layer. On top of the second ash layer occurs another ca. 45 cm thick lapilli layer that is missing in Q2.

4.2. Off-axis section

The tephra deposits that are outside the main dispersal axis to the East and the West of La Vache and Lassolas differ from the deposits along the dispersal axis. The off-axis section (Q3) is located ca. 2 km to the East of Lassolas. It is ca. 60 cm thick and is overlying older volcanic deposits (Fig. 5). The section lacks both the granitic lithic-rich basal layer and the characteristic stratigraphic layering of the proximal and distal sections; instead it is formed by a single massive layer consisting of fine lapilli-sized highly vesicular scoria. A gradual change from the massive off-axis section to the layered along axis sequence was observed in the western part of the field area. A temporary deep track exposed the sequence on a transect oblique to the dispersal axis. In the direction of the dispersal axis the first layer to appear underneath the off-axis deposit is L1. Further towards the dispersal axis the off-axis section is thinning and two more layers appear underneath. The last layers to appear are the two ash layers at the top.

5. Tephra dispersal pattern and volume estimates

We assume that the tephra was erupted simultaneously from both cones, because we do not have any field evidence to prove that the two cones were active at different times. This is supported by the isopach map of the total tephra deposit (Fig. 8a) and by the isopach maps of the three different eruption phases (Fig. 8b,c and d). Fig. 8a shows a dominant dispersion to the south. The isopach maps of the first three layers (L1, L2, L3) confirm this dispersion (Fig. 8b and c). However, Fig. 8d shows that material near the top of the tephra sequence was dispersed towards the East.

Most approaches to estimate the volume of a tephra blanket are based on the relationship of the thickness T to the tephra-covered area, where the relationship of the volume V to the square root of the isopach area A can be described by the thickness decay rate as the following (Bonadonna and Costa, 2012; Daggitt et al., 2014):

$$V = \int_0^\infty \mathrm{TdA} = \int_0^\infty \mathrm{Tdx}^2 = \int_0^\infty \mathrm{T}(x)x\,dx. \tag{2}$$

The total volume of the La Vache and Lassolas tephra deposit was calculated on the basis of the combined isopach map using the online VHub AshCalc tool by Daggitt et al. (2014). The $\ln(T)$ vs. $\sqrt{A}$ plot in Fig. 9 shows that the data can be linearly fitted by the two segment exponential model of Fierstein and Nathenson (1992) and Pyle (1995). The exponential thickness decay is calculated for each segment using the following equation (Pyle, 1995), with k being a constant and T_0 being the extrapolated maximum thickness at the vent for $A = 0$:

$$T = T_0\, exp\left(-k\sqrt{A}\right). \tag{3}$$

The minimum calculated total volume for the La Vache and Lassolas tephra is 56×10^6 m ^{3}, using a two segment exponential model (Fierstein and Nathenson, 1992).

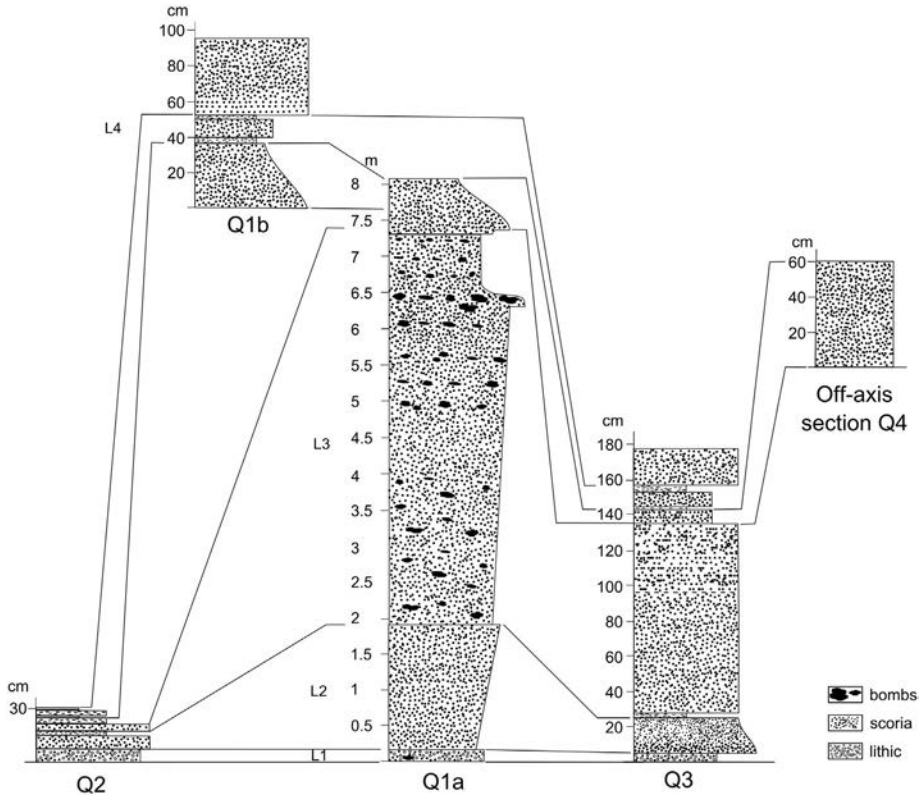

Fig. 5. Correlation of four sections of the tephra fall deposit, with section Q3 in the North East and section Q2 in the South West. Section Q1 has a different scale as the result of its large thickness.

6. Vertical stratigraphic variations of grain size, density and componentry

6.1. Variations in grain size and density

In Q1a the median grain size increases continuously from -0.5ϕ in L1 to -3.0ϕ at the top of L2 (Fig. 10, Table 1) and drops to -2.4ϕ at the base of L3. The median grain size is constant throughout L3 and drops again to -1.6ϕ in layer L4, with a further decrease in the median grain size towards the top of the section.

The mean density of the juvenile clast decreases continuously from layer L1 (1340 kg/m ^{3}) to the base of L3 (1010 kg/m ^{3}). However, the mean clast density increases continuously throughout L3 to 1260 kg/m ^{3} at the top (Fig. 10, Table 1). In contrast, in L4 the mean density is 960 kg/m ^{3} and changes to 1270 kg/m ^{3} in the topmost layer (Fig. 10).

6.2. Variations in the componentry

Spiny scoria and rounded scoria form the two main components. Their relative proportions correlate negatively throughout the sequence (Fig. 10). L1 contains lower amounts of spiny scoria (10 vol.% in the ash fraction and 50 vol.% in the lapilli fraction) and higher amounts of rounded scoria (40 vol.% in the ash fraction and 60 vol.% in the lapilli fraction) compared to the main sequence (L2 and L3) that contains ca. 90 vol.% of spiny scoria and less than 10 vol.% of rounded scoria. This ratio changes significantly within L4 ash fraction that contains 62 vol.% of spiny scoria and 34 vol.% of rounded scoria. However, the ratio of spiny to rounded scoria does not change in the lapilli fraction. In the top layer the amounts of spiny and rounded scoria are similar to the values in L1.

The amount of free crystals is low (<1 vol.%) and constant in the lapilli fraction over the entire sequence. In the ash fraction the amount of free crystals varies within the stratigraphy between 2 and 6 vol.%. Again the amount of free crystals changes between L1 (5 vol.%) and L2 (3 vol.%). It increases further to 6 vol.% in the middle part of L2 and drops to 4 vol.% at the top. At the bottom of L3 the amount of free crystals slightly increases to 6 vol.% and it decreases throughout L3 to 2 vol.% in the lower part of L4. In the top part of the sequence the amount of free crystals increases continuously again to 7 vol.%.

The high amount of lithic clasts is characteristic for L1, as it gives the layer a white-spotted appearance. In the lapilli fraction the amount of lithic clasts is 5 vol.%, whereas it is 23 vol.% in the ash fraction (Fig. 10). The amount of lithic clasts drops to <1 vol.% in L2 and remains constant at this low value over the entire sequence. In the topmost layer, however, the amount of lithic clasts in the lapilli fraction increases again to 4 vol.%.

7. Total volcanic budget

The bulk volume of the eruption ejecta and their dense rock equivalent (DRE) were determined for the two scoria cones, the lava flow and the tephra deposit. Assuming simple cone shapes with dimensions given earlier, the two scoria cones have together a bulk volume of 29×10^6 m ^{3} with a DRE of 17×10^6 m ^{3} (Table 2). For the lava flow the bulk volume and the DRE were determined separately for the dense part of the lava (20 m thick) and the scoriaceous rubble part (10 m thick). The dense part has a total bulk volume of 338×10^6 m ^{3}, while the scoriaceous rubble layer associated with the lava flow has a total bulk volume of 134×10^6 m^3 with a DRE of 79×10^6 mm ^{3}. In addition, the volume of the tephra determined in this study is 56×10^6 m^3 and a DRE of 30×10^6 mm ^{3}. The total bulk volume of the whole eruption is thus in the order of 547×10^6 m^3 with a DRE of 454×10^6 m^3.

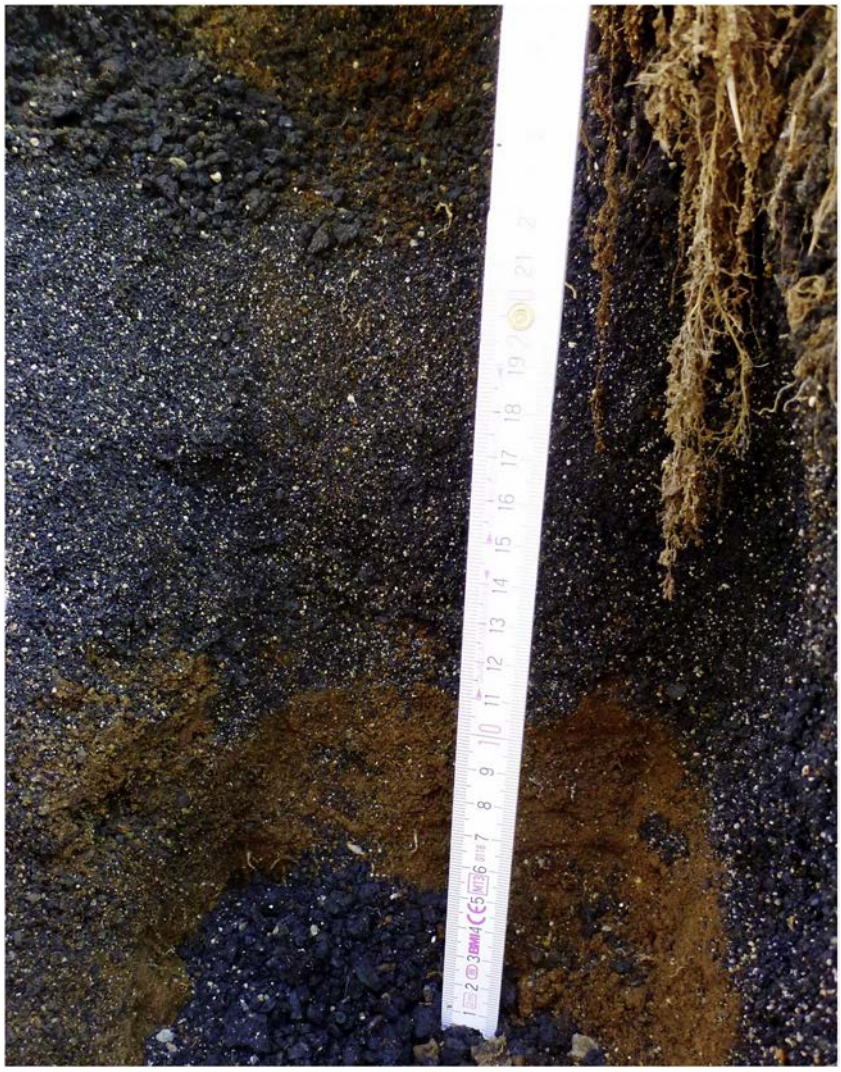

Fig. 6. Close-up of L1 overlying brown older volcanic deposit and underlying the coarser grained L2 layer. L1 is characterised by the high abundance of white lithic clasts, the well sorting and its finer grain size.

8. Discussion

8.1. Interpretation of the different clast types

8.1.1. Juvenile clasts

The poorly vesicular, rounded scoria is similar to the subrounded black scoria described in Mexico at Parícutin by Pioli et al. (2008) and at Jorullo by Rowland et al. (2009). In both studies these rounded clasts are interpreted as fragments of relatively degassed magma. The round shape is generally explained to be the result of surface tension relaxation of the magma that pulls the molten fragments up into spheres after fragmentation (Alvarado et al., 2011 and references therein). This is supported by the presence of single phenocrysts in the interior of many of the rounded scoria at La Vache and Lassolas that may have acted as a nucleus around which the melt contracted. On the other hand, the round shape could be also the result of abrasion and milling processes in the vent. However, no signs of abrasion such as pitting and scouring were observed on the surface of the rounded scoria from La Vache and Lassolas, ruling out abrasion as the main process determining the shape of these clasts. The spiny scoria was formed at the same time by fragmentation of vesiculated magma. D'Oriano et al. (2011) observed crystal-rich, dense juvenile clasts coexisting with very vesicular, glassy juvenile clasts in the deposits of ash-dominated eruptions at Vesuvius and suggested that this clast assemblage is the result of lateral and/or vertical variations of vesicularity and crystal content in the ascending magma body. Gurioli et al. (2015 and references therein) describe different conduit processes that lead to water depletion in the magma including bubble collapse and coalescence and the transition from closed- to open-system degassing. The platy, curviplanar, sheet like juvenile fragments are similar to flat clasts, named pajaritos by Pioli et al. (2008) and to the plate tephra formed during the 2008–2009 Llaima eruption and described in detail by Ruth and Calder (2014). The latter explain the formation of these fragments with the rupturing of large gas slugs at the surface of the magma column, where the sheet like fragments are the remnants of the ruptured slug wall. Therefore the presence of these clasts within the entire La Vache and Lassolas tephra would indicate that single large gas slugs were able to rise to the top of the magma column, where they ruptured. The rise of gas slugs and their individual bursting have been traditionally considered to occur during low intensity, Strombolian style activity (e.g. Parfitt, 2004; Harris and Ripepe, 2007). The presence of the platy tephra also in the distal sections, however, indicates that it was formed also during very explosive phases of the eruption driven by magma fragmentation.

8.1.2. Lithic material

Accidental lithic material is only present in the La Vache and Lassolas tephra deposit in L1 and in small amounts at the top of L4. Large

Fig. 7. The image shows 4 m of L3 in the proximal Q1 section with the massive structure of the layer and the train of larger bombs in the top part of L3.

amounts of accidental lithic material within pyroclastic deposits at monogenetic volcanoes are commonly considered to be the result of highly energetic phreatomagmatic explosions caused by violent magma/water interaction (e.g. Funiciello et al., 1976). However, our data on the structure of L1 and the textures of the other components yield evidence for a dominantly magmatic fragmentation process.

The production of large amounts of fine ash is characteristic of explosive magma/water interaction, where the magma is fragmented during molten fuel coolant interaction (MFCI) explosions into particles smaller than 130 μm (Zimanowski et al., 1991; Büttner et al., 2002). However, the amount of fine ash smaller 130 μm is less than 10 wt.% even in the relatively distal L1 samples. In addition, L1 has the same grain size in both proximal and distal sections, indicating that the scarcity in fine ash in the proximal section is not the result of wind elutriation. The similar grain size in the proximal and distal sections rather suggests that no fine ash was produced during the eruption. The clean surfaces of both lithic and juvenile material also indicate that this material was not produced by phreatomagmatic explosions, because ash coating of clasts is a characteristic of phreatomagmatic deposits and should be present if this material was formed by classical phreatomagmatic explosions. In addition, juvenile clasts formed by phreatomagmatic eruptions have typically blocky, equant shapes with planar or curviplanar fracture surfaces (Wohletz, 1983; Rowland et al., 2009), which were not observed on the juvenile clasts of La Vache and Lassolas. Furthermore, the pulsatory character of phreatomagmatic eruptions would lead to the deposition of finely layered deposits as can be observed at different maar volcanoes such as the Fekete-hegy maars, Hungary (Auer et al., 2007) or the Lake Purrumbete maar, Australia (Jordan et al., 2013). L1, however, is a massive 15 cm thick layer, with no indication of layering, that formed from steady fall out of a sustained eruption column. This suggests that the lithic material was not generated by phreatomagmatic eruptions.

We suggest that the lithic material is the result of upper conduit erosion at the onset of the eruption and subsequent incorporation in the eruptive jet rushing up to the surface. At the beginning of the eruption conduit erosion may be large due to conduit wall collapses which are caused by catastrophic stress changes within the conduit walls (Mitchell, 2005). However, we cannot discard the presence of some groundwater that may have been vaporised to steam in the conduit walls, thus favorizing lithic grain detachment from the hosting granite, but this was not the main driving process of this highly energetic eruption.

8.2. Onset of the eruption

Lithic-rich basal layers are typical of cone-forming eruptions in the Chaîne des Puys and have been commonly interpreted at La Vache

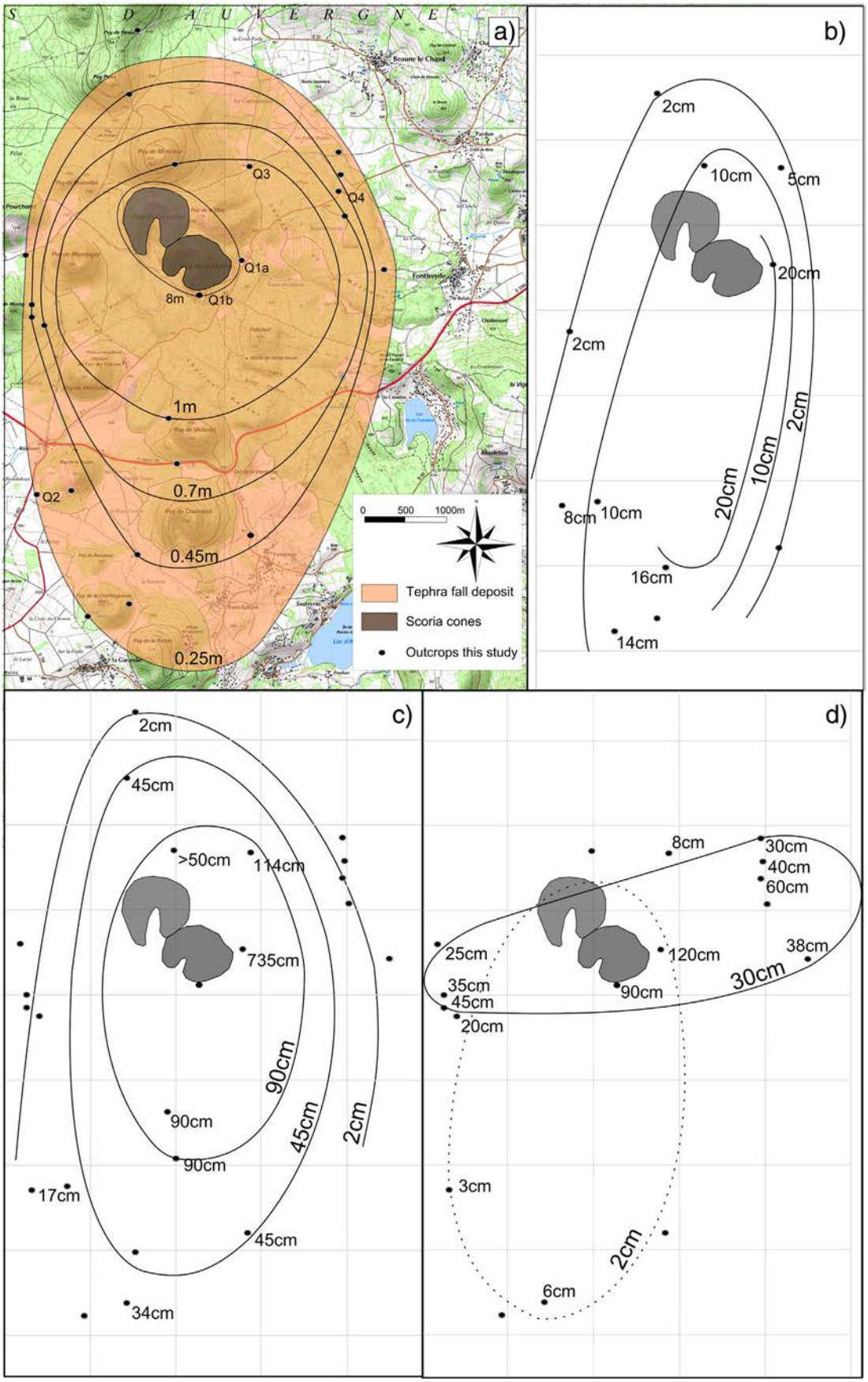

Fig. 8. Isopach maps for a) the total tephra deposit, b) the opening phase layer PL1, c) the second and third phase of the eruption (layer PL2 and PL3) and d) the main layer of the fourth phase (layer PL4).

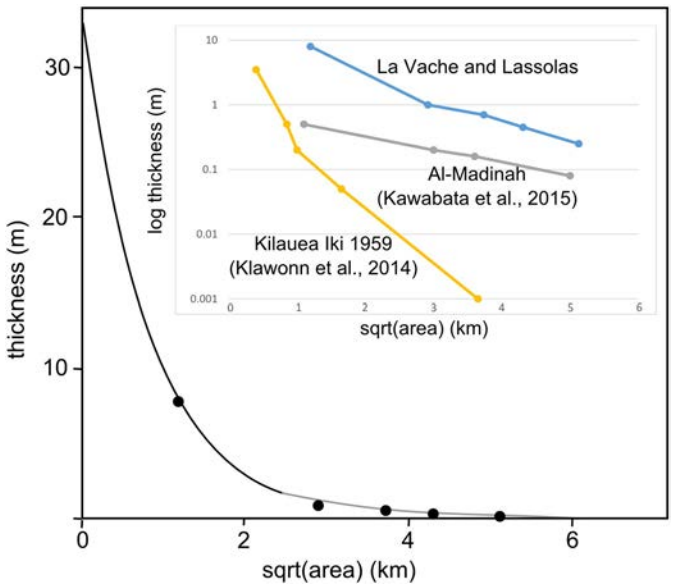

Fig. 9. This graph shows the good fit of the data to the two segments used in the exponential model. The fitting of the data to the segments and the calculation of the volume was done using the online VHub AshCalc tool by Daggitt et al. (2014). Plotting the data together with data of the Kilauea Iki 1959 eruption (Klawonn et al., 2014) and of the Al-Madinah eruption (Kawabata et al., 2015) indicates the larger volume of tephra produced by the La Vache and Lassolas eruption.

and Lassolas and elsewhere as the result of an initial phreatomagmatic opening phase (Hardiagon et al., 2011; Delcamp et al., 2014) that has also been suggested for the formation of the La Vache and Lassolas basal layer (Miallier, 2014, personal communication). However, as discussed above, the driving process for the eruption of L1 was not phreatomagmatic, although it was very energetic as evidenced by the relative fine grain size of the material (coarse ash) even in near vent locations, which indicates that the small grain size is the result of intensive fragmentation rather than of abrasion and sorting during transport (Palladino and Taddeucci, 1998; Colucci et al., 2013). We suggest that during the first erupting phase the magma was fragmented by a high strain rate in a gas jet that was also eroding the conduit walls. The gas may have accumulated at the tip of the dyke prior to eruption during dyke emplacement (Carrigan, 2000). Menand and Tait (2001) demonstrated in their experimental work that at the tip of a vertical ascending dyke a gas pocket forms that increases the velocity of the fissure opening. The difference in the ascent velocity of the gas pocket to the main dyke can result in the separation of the gas pocket from the dyke, with the gas pocket being able to carry a small volume of magma dispersed as small fragments of magma within the gas. Menand and Tait (2001) further suggested that the eruption of this gas pocket is the reason for precursory volcanic activity before many large eruptions. The ascent and eruption of such a gas pocket may well explain the formation of L1. A different explanation for the formation of L1 would be that the ash sized fragments were produced by ripping of little pieces from a low viscosity magma body by a continuous gas flow through a permeable top part of the magma column, as has been suggested by D'Oriano et al. (2011) for the formation of ash-dominated eruptions at Vesuvius.

8.3. Timing of the formation of the cones, the lava flow and the tephra deposit

After the first vent clearing, gas driven eruptive phase, the activity continued with highly energetic eruptions of predominantly vesicular juvenile material that produced the thickest layer, reaching 8 cm 3.4 km from the vent, suggesting the formation of a stable eruption column and plume (Fig. 11). During this phase the eruption intensity continuously increased with a corresponding increase in the column height, as evidenced by the reversed grading of the L2 layer. This gradation pattern is present in all sections along the dispersal axis, also in up-wind section Q3, indicating that it is not the effect of wind shift. An increase in the eruption intensity is also supported by a continuous decrease in the mean clast density, which indicates an increase in the volume of the gas phase prior to fragmentation. The very low amount of rounded scoria also demonstrates that there was only a

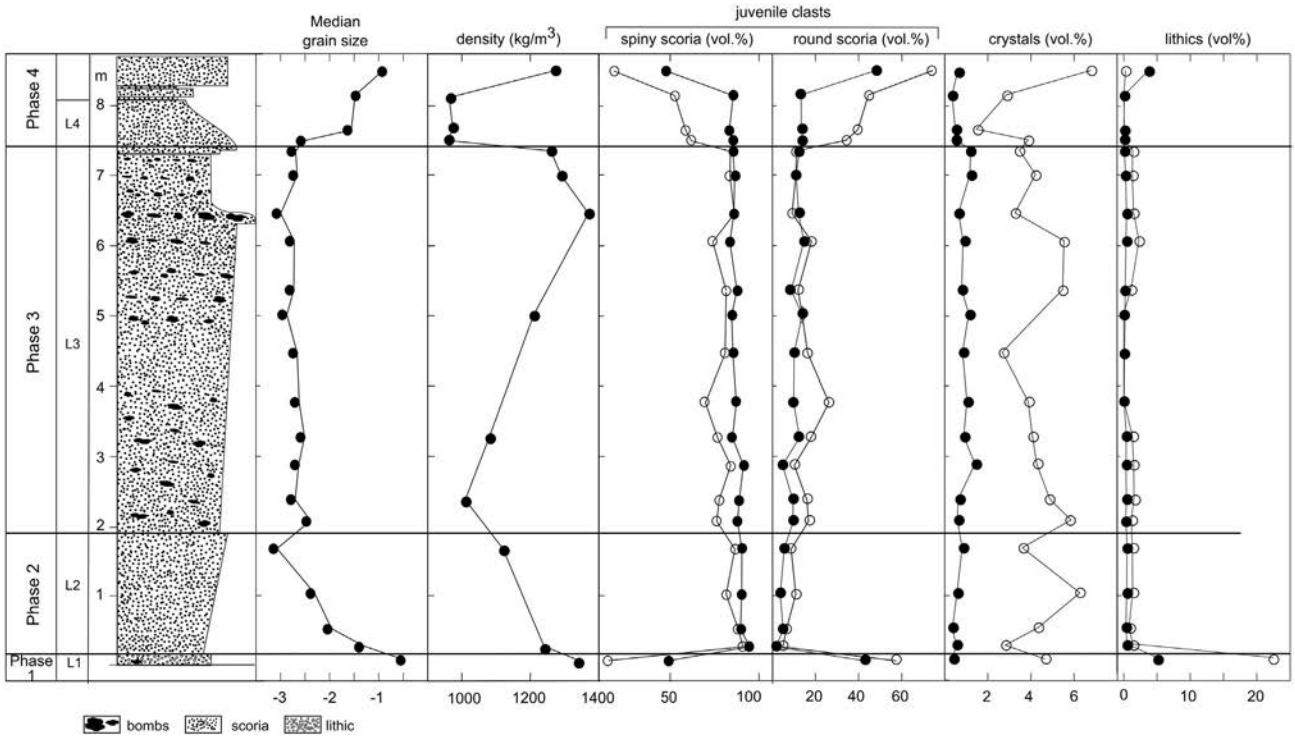

Fig. 10. Variations of median grain size, the main four clast components and the mean clast density within the proximal stratigraphic succession of the La Vache and Lassolas tephra deposit.

Table 1
Data table including the results of all analysis for each sample with the coordinates of the sample location.

Sample	Coordinates	Md	Lapilli size fraction (vol.%)					Ash size fraction (vol.%)				Mean density
	Lambert 2 etendu	ϕ	Spiny	Round	Flat	Crys	Lith	Spiny	round	Crys	Lith	(kg/m^3)
Q1a-11	649300/2078475	−2.69	85.42	12.86	0.34	1.2	0.19	83.87	11.33	3.47	1.33	1260
Q1a-10d	649300/2078475	−2.66	86.31	11.07	1.2	1.17	0.26	83.63	10.89	4.21	1.27	1290
Q1a-10b	649300/2078475	−3.00	85.85	12.16	0.95	0.64	0.41	86.08	9.19	3.27	1.47	1370
Q1a-9c	649300/2078475	−2.72	83.58	14.62	0.63	0.85	0.32	74	18.2	5.53	2.27	
Q1a-9b	649300/2078475	−2.73	87.55	8.8	2.65	0.79	0.21	81.53	11.93	5.47	1.07	
Q1a-9a	649300/2078475	−2.87	84.63	13.84	0.24	1.11	0.17	–	–	–	–	1210
Q1a-8f	649300/2078475	−2.67	85.32	10.13	3.62	0.83	0.11	80.93	16.4	2.67	0	
Q1a-8e	649300/2078475	−2.62	87.2	9.92	1.81	1.03	0.04	69.87	26.27	3.87	0	
Q1a-8d	649300/2078475	−2.51	85.07	12.61	1.07	0.89	0.37	76.67	18	4.07	1.27	1080
Q1a-8c	649300/2078475	−2.63	91.18	4.81	2.3	1.4	0.32	84.07	10.2	4.27	1.47	
Q1a-8b	649300/2078475	−2.7	88.91	9.58	0.49	0.63	0.39	77.53	16.07	4.87	1.53	1010
Q1a-8a	649300/2078475	−2.39	87.92	9.68	1.53	0.58	0.29	76.25	16.77	5.86	1.13	1150
Q1a-7	649300/2078475	−3.07	90.37	5.54	2.79	0.81	0.49	86.4	8.73	3.6	1.27	1120
Q1a-6	649300/2078475	−2.56	–	–	–	–	–	–	–	–	–	
Q1a-5	649300/2078475	−2.3	90.28	3.68	5.04	0.57	0.43	81.53	10.87	6.27	1.33	
Q1a-4	649300/2078475	−2.3	–	–	–	–	–	–	–	–	–	
Q1a-3	649300/2078475	−1.96	89.57	5.01	4.75	0.36	0.31	88.33	6.53	4.33	0.8	
Q1a-2	649300/2078475	−1.31	94.8	1.77	2.44	0.52	0.47	91	4.87	2.8	1.33	1240
Q1a-1	649300/2078475	−0.47	49.32	43.12	2.14	0.37	5.04	15.2	57.6	4.67	22.53	1340
Q1b-5	648975/2078300	−9.92	47.43	48.08	0.14	0.61	3.74	18.52	74.42	6.80	0.27	
Q1b-4	648975/2078300	−1.48	85.49	13.37	0.72	0.34	0.08	52.60	44.53	2.87	0.00	
Q1b-3	648975/2078300	−1.53	83.27	13.47	2.77	0.49	0.00	58.80	39.67	1.47	0.07	
Q1b-2	648975/2078300	−1.56	85.19	13.38	0.88	0.47	0.07	61.87	34.20	3.87	0.07	
Q1b-1	648975/2078300	−2.51	85.42	12.86	0.34	1.20	0.19	83.87	11.33	3.47	1.33	
Q2-6	646800/2075650	−0.49	–	–	–	–	–	–	–	–	–	
Q2-5	646800/2075650	0.09	–	–	–	–	–	–	–	–	–	
Q2-4	646800/2075650	−1.30	94.62	3.75	0.82	0.61	0.20	87.59	9.94	2.27	0.20	
Q2-3	646800/2075650	−0.77	–	–	–	–	–	–	–	–	–	
Q2-2	646800/2075650	−1.91	95.59	1.96	1.69	0.76	0.00	88.67	6.07	3.60	3.60	
Q2-1	646800/2075650	−0.42	43.74	49.48	0.78	0.96	5.04	13.60	57.73	2.40	2.40	
Q3-6	0497736/5062455	−1.72	–	–	–	–	–	–	–	–	–	
Q3-5	0497736/5062455	0.00	–	–	–	–	–	–	–	–	–	
Q3-4	0497736/5062455	−0.79	83.34	14.49	1.74	0.38	0.05	51.33	45.27	3.33	0.07	
Q3-3e	0497736/5062455	−2.20	90.97	6.49	1.61	0.85	0.09	80.60	15.67	3.60	0.13	
Q3-3d	0497736/5062455	−2.01	78.69	14.77	5.18	1.08	0.28	58.53	36.00	5.07	0.40	
Q3-3c	0497736/5062455	−2.09	78.90	14.56	3.53	1.56	1.45	54.18	35.34	8.02	2.47	
Q3-3b	0497736/5062455	−2.05	89.46	6.43	3.30	0.73	0.09	85.27	7.93	6.00	0.80	
Q3-3a	0497736/5062455	−1.41	59.12	36.65	0.43	1.12	2.68	43.13	40.93	6.67	9.27	
Q3-2	0497736/5062455	−2.23	93.26	3.15	3.04	0.51	0.04	83.33	11.67	4.47	0.53	
Q3-1	0497736/5062455	−0.24	25.59	58.66	0.10	0.39	15.26	7.27	55.13	1.80	35.80	

very small proportion of gas-poor material in the conduit. The two scoria cones probably began already to form during this phase of the eruption by direct fall out from the lower part of the eruption column, as has been suggested by Valentine et al. (2005) for the construction of scoria cones related to extensive tephra deposits such as the La Vache and Lassolas cones.The two separate cone edifices indicate that each cone had probably developed its own eruption column that may have merged together at a higher altitude. The second phase ended with a climax in explosive intensity at the top of L2.

The third phase of the eruption is characterised by stable eruption conditions, evidenced by the constant componentry, median grain size and grain size distribution in L3 and its thickness. On the basis of field observations, we interpret that the extrusion of lava started simultaneously with the ejection of L3 (Fig. 11). Both the continuous extrusion of lava and the constant ejection of tephra, indicate continuous magma supply and an efficient process of degassing and separation of gas-rich and gas-poor material. This phase was probably also the main cone forming phase, but the continuous effusion of lava through the openings in the cones prevented their closure. Simultaneous formation of lava and tephra has been documented at several scoria cones such as Irao volcano, Japan (Kiyosugi et al., 2014), the scoria cones of the AD 1256 eruption in Saudi Arabia (Kawabata et al., 2015), Jorullo (Rowland et al., 2009), Parícutin (Pioli et al., 2008, 2009) and Etna (Behncke et al., 2006). Evidence for the onset of the lava flow formation after a first cone forming phase at la Vache and Lassolas is given by the scoria raft that can be found several kilometres down the lava flow. The location outside the main lava channel indicates that this raft was transported at an early stage of the lava flow emplacement, before the formation of the main lava channel. Pioli et al. (2009) suggest that simultaneous effusive and explosive activity is the result of magma separating into a gas-rich phase and a liquid phase within the conduit that are then divided into vertical and lateral branches of the conduit system. Menand and Phillips (2007) demonstrated that effective gas segregation occurs in horizontal branches of a plumbing system, where the magma is stored for a short time and separates into a gas-rich foam like phase and a gas-poor phase. Both phases flow back into the conduit and erupt together with the ascending melt in the main conduit. Taking this model into account for the eruption of La Vache and Lassolas, the onset of lava effusion may be the result of the formation of a shallow horizontal intrusion and effective gas segregation within this intrusion.

Table 2
Values for the covered area, the volume and the dense rock equivalent (DRE) of the different eruption products of the La Vache and Lassolas eruption.

	Area (m^2)	Volume (m^3)	DRE (m^3)
Cones	1×10^6	29×10^6	17×10^6
Tephra	30×10^6	56×10^6	30×10^6
Lava flow			
Dense part	16.38×10^6	328×10^6	328×10^6
Rubble	16.38×10^6	134×10^6	79×10^6
Total		547×10^6	454×10^6

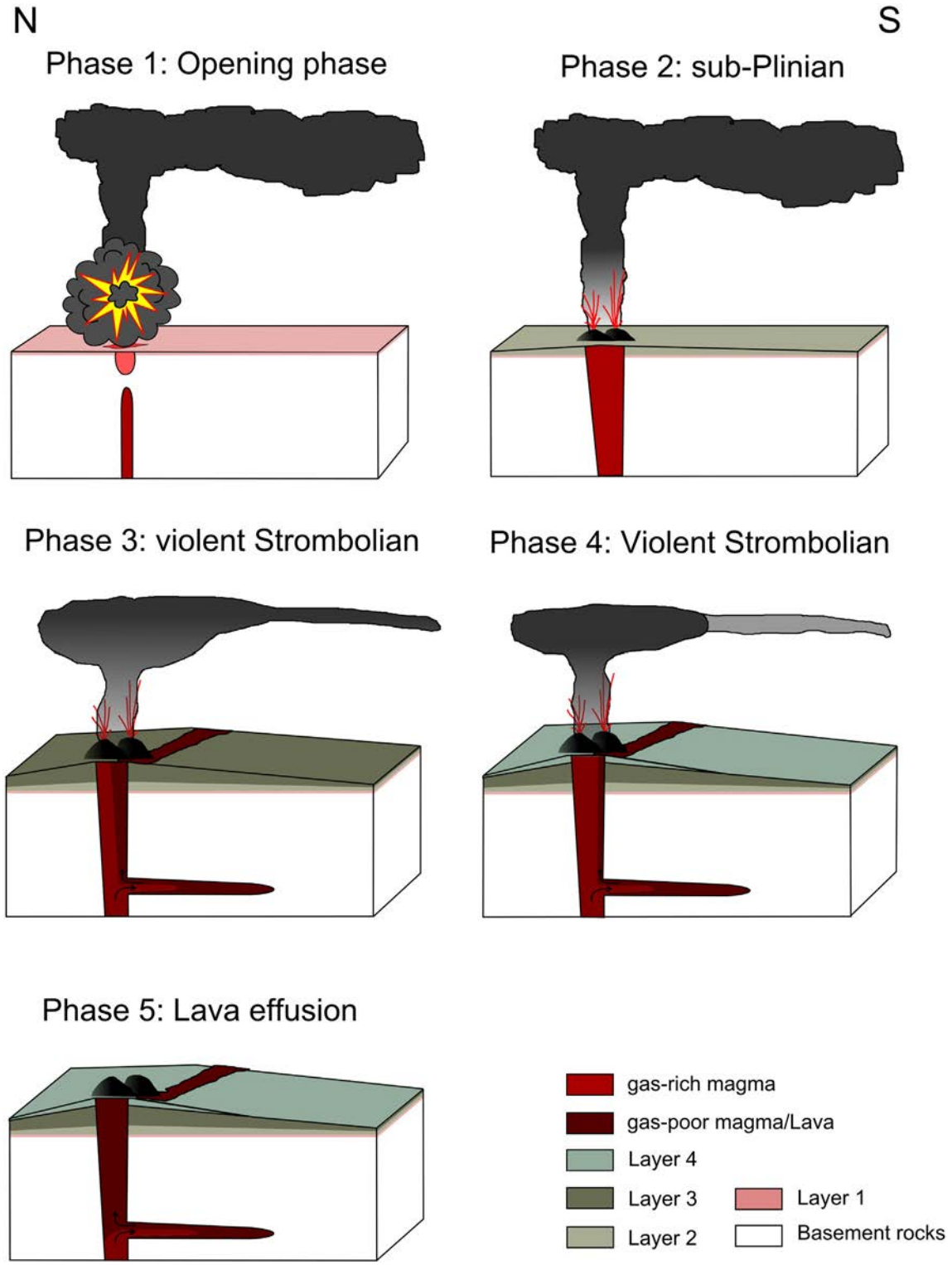

Fig. 11. Evolution of the eruption from a gas-driven explosive first vent opening phase, to a highly explosive cone-forming second phase, to less explosive violent Strombolian third and fourth phase and quiet lava effusion in the last phase of the eruption.

Intrusions within the shallow plumbing system of monogenetic volcanoes were observed in different volcanic fields such as the Lunar Crater volcanic field, Nevada (Hintz and Valentine, 2012), the Hopi Buttes Volcanic Field, Arizona (Re et al., 2015), and at Lemptégy scoria cone in the Chaîne des Puys, France (Delcamp et al., 2014). The intrusions form due to overpressure in the main conduit and local stresses caused by the loading of the volcanic edifice (Hintz and Valentine, 2012; Re et al., 2015). Therefore, the formation of shallow horizontal intrusions at the La Vache and Lassolas cone complex may be the result of the growth of the two scoria cones at the surface. The existence of shallow intrusions beneath scoria cones has also been suggested by Johnson et al. (2008) for degassing and crystallisation of the Jorullo melts and has been observed by Valentine and Krogh (2006) at an eroded cinder cone in the Paiute Ridge area of southern Nevada.

After gas segregation in the shallow intrusion, both gas-rich and gas-poor phases may rise together in the conduit and may only separate in

the very shallow top part of the plumbing system where the gas-poor material is feeding into the lava flow and the gas-rich material is erupting in violent Strombolian explosions as suggested by Pioli et al. (2009). The gas-rich phase may escape from the intrusion, where it separated, as large gas slugs, that burst at the surface forming the platy tephra. Therefore the platy tephra may not only form during phases of low intensity as has been suggested by Ruth and Calder (2014), but also by efficient gas segregation in a complex plumbing system.

The increase in the mean clast density during this phase is correlated to the decrease in magma vesicularity, and may indicate a continuous decline of the eruption. An influence of post-depositional processes such as bubble collapse can be ruled out because the measured clasts are small enough to have been cooled during flight (Guilbaud et al., 2009). In addition, many clasts broke by the impact with the ground on landing, which indicates brittle behaviour and thus complete solidification prior to deposition (Guilbaud et al., 2009). A general decrease in vesicularity was also observed by Di Traglia et al. (2009) in the violent Strombolian deposits of the Croscat scoria cone, Spain, and interpreted as evidence for a progressive decline of the eruption intensity. Waning of the eruption is also supported by the presence of non-juvenile granitic material included in the juvenile material in the upper part of L3. A decline in the eruption rate may cause a deepening of the fragmentation level or a decrease in the flow pressure within the feeding system resulting in conduit wall failure (Mitchell, 2005) and incorporation of the lithic material into the magma.

The main dispersal axis of eruption phase 1–3 is to the south, with no indication that the wind direction shifted in this time. The predominant wind direction nowadays is to the east and wind directions to the south are relatively rare and unstable and occur only for a few days in a row. Thus, the uniform dispersal axis indicates that the deposits of phase 1–3 were deposited in a relatively short time frame.

The stable conditions of eruption phase 3 ended at the top of L3 and a new phase started with the eruption of L4. This phase may have been caused by an abrupt increase in the magma ascent rate caused by a fresh, gas-rich magma pulse as suggested by the very low mean clast density (880 kg/m ^{3}) and the lowest amount of free crystals (1.4 vol.%) observed within the whole La Vache and Lassolas succession. The very low mean clast density implies that the magma was highly vesiculated. This high degree of vesiculation reduces the material strength of the magma (Heap et al., 2014), which may be the reason why the magma fragmented into smaller particles than before. A similar renewal in the eruption intensity as the result of the arrival of a new magma batch has been suggested by Erlund et al. (2010) for the second phase of the Parícutin eruption. In addition, the increased amount of rounded scoria may be again the result of clearing out of more degassed material from the conduit at the beginning of this new eruption phase. The presence of several thin ash layers intercalated with thin lapilli horizons in the top part of the section may be interpreted as a decrease in the explosive activity (Erlund et al., 2010), but they are rather the result of wind shift effects and the deposition of the coarser material to the east forming the off-axis deposit. The large increase in the amount of rounded scoria (74 vol.% in the ash fraction) and in the amount of free crystals (6.8 vol.% in the ash fraction) in the topmost layer, together with the increase in the mean clast density (1270 kg/m ^{3}) indicate that the magma became more and more degassed again towards the end of the explosive phase. This can be explained by a decrease in the magma ascent rate leading to an increase in degassing of the magma in general prior to fragmentation. The model of Menand and Phillips (2007) predicts that low magma ascent rates cause the eruption of gas-poor material, because the gas segregation rate is higher than the magma supply rate and therefore the fresh ascending magma is predominantly stored in the intrusions and mostly degassed material from the intrusion will ascent to the surface. This may explain the transition from explosive to dominantly effusive activity at the end of phase 4 (Fig. 11), which is in agreement with the observations of Di Traglia et al. (2009) at the Croscat scoria cone and of Pioli et al. (2008, and reference therein) at Parícutin.

A comparison of the material volumes of explosive activity (cones + tephra deposit) to the material volume of effusive activity (lava flow) shows that the effusive volume is nine times larger than the explosive ejecta volume, implying that gas segregation and gas loss were effective during the eruption and was probably the main eruption-controlling process.

9. Conclusions

This study presents the results of detailed field and tephra studies on a highly explosive eruption of the monogenetic La Vache and Lassolas scoria cone complex, giving insights into the complex eruption history and the control of the plumbing system on the eruption. Our results demonstrate that lithic-rich tephra deposits are not necessarily the result of phreatomagmatic eruptions, but can also be formed by the eruption of a gas-dominated phase. This shows that care has to be taken with the interpretation of lithic-rich tephra fall deposits, because lithic material is not a precise indicator for phreatomagmatic activity, and therefore more detailed analysis of the material is needed to determine the eruption type. Our findings show that a gas-rich phase can separate from the ascending magma body and can erupt in a highly explosive way, opening the vent and producing large amounts of finely fragmented lithic material.

In addition, this study suggests that the eruption type and behaviour are strongly dependent on subsurface processes such as the ascending dyke and the following evolution of the plumbing system. The formation of shallow intrusions may lead to effective gas segregation from the magma and the eruption of both gas-poor and gas-rich magma, as described by Menand and Phillips (2007). However, the ratio of gas-poor to gas-rich magma is also dependent on the magma ascent rate. If this rate is higher than the rate of gas segregation within the intrusion, gas-rich magma will predominate in the conduit and vice versa (Menand and Phillips, 2007). The observed changes in the eruption intensity during the La Vache and Lassolas eruption can be well explained by the interplay of the magma ascent rate and the process of gas segregation within a shallow intrusion.

The eruption of the La Vache and Lassolas cone complex started out with highly explosive activity that covered a wide area of at least 30 km ^{2} with an at least 20 cm thick tephra layer. The intensity decreased after the first two eruption phases to violent Strombolian type eruptions with the simultaneous eruption of tephra and a lava. The lava effusion continued after the end of the explosive phase and formed a 22 km-long flow. This deposit demonstrates that even cone-forming eruptions can be highly explosive and that they can affect a large area surrounding the vent. This is very important to keep in mind when dealing with the hazard assessment of possible scoria cone eruptions.

Acknowledgements

This research was financed by the French Government Laboratory of Excellence initiative n° ANR-10-LABX-0006, the Région Auvergne and the European Regional Development Fund. This is Laboratory of Excellence ClerVolc contribution number 191. We thank the Région Auvergne and the FEDER for the financial support of this project in the form of financing the position of S.C. Jordan. We also thank Baptiste Haddadi for his great help with the field work, Didier Laporte for his support on the project and Didier Miallier for his age data of the La Vache and Lassolas eruption.

References

Alvarado, G., Pérez, W., Vogel, T., Gröger, H., Patiño, L., 2011. The Cerro Chopo basaltic cone (Costa Rica): an unusual completely reversed graded pyroclastic cone with abundant low vesicular cannonball juvenile fragments. J. Volcanol. Geotherm. Res. 201, 163–177.

Auer, A., Martin, U., Németh, K., 2007. The Fekete-hegy (Balaton Highland Hungary) "soft-substrate" and "hard-substrate" maar volcanoes in an aligned volcanic complex—implications for vent geometry, subsurface stratigraphy and the palaeoenvironmental setting. J. Volcanol. Geotherm. Res. 159, 225–245.

Barker, S., Rotella, M., Wilson, C.J.N., Wright, I., Wysoczanski, R., 2012. Contrasting pyroclast density spectra from subaerial and submarine silicic eruptions in the Kermadec arc: implications for eruption processes and dredge sampling. Bull. Volcanol. 74, 1425–1443.

Baudry, D., Camus, G., 1969. Observations sur les recouvrements volcaniques entre le puy de pariou et le puy de la vache. Rev. Sci. Nat. Auvergne 35, 45–48.

Behncke, B., Neri, M., Pecora, E., Zanon, V., 2006. The exceptional activity and growth of the Southeast Crater, Mount Etna (Italy), between 1996 and 2001. Bull. Volcanol. 69, 149–173.

Boivin, P., Thouret, J., 2013. The volcanic Chaîne des Puys: A unique collection of simple and compound monogenetic edifices. In: Fort, M., André (Eds.), Landscapes and Landforms of France, nineth ed. Springer, Heidelberg, pp. 81–91.

Boivin, P., Besson, J., Briot, D., Camus, G., De Goër de Hervé, A., Gourgaud, A., Labazuy, P., Langlois, E., de Larouziére, F., Livet, M., Mergoil, J., Miallier, D., Morel, J., Vernet, G., Vincent, P., 2009. Volcanologie de la Chaîne des Puys Massif Central Français. fifth ed. 1. Parc Naturel Régional des Volcans d'Auvergne, p. 25000.

Bonadonna, C., Costa, A., 2012. Estimating the volume of tephra deposits: a new simple strategy. Geology 40 (5), 415–418.

Büttner, R., Dellino, P., La Volpe, L., Lorenz, V., Zimanowski, B., 2002. Thermohydraulic explosions in phreatomagmatic eruptions as evidenced by the comparison between pyroclasts and products from Molten Fuel Coolant Interaction experiments. J. Geophys. Res. 107 (B11).

Camus, G., 1975. La Chaîne des Puys (Massif Central français). Etude Structural et Volcanologique. University Clermont-Ferrand (Ph.D. thesis).

Carrigan, C.R., 2000. Plumbing systems. In: Sigurdsson, H., Houghton, B., McNutt, S., Rymer, H., Stix, J. (Eds.), Encyclopedia of Volcanoes. Academic Press, pp. 219–235.

Cimarelli, C., Di Traglia, F., Taddeucci, J., 2010. Basaltic scoria textures from a zoned conduit as precursors to violent strombolian activity. Geology 38 (5), 439–442.

Colucci, S., Palladino, D., Mulukutla, G., Proussevitch, A., 2013. 3-d reconstruction of ash vesicularity: insights into the origin of ash-rich explosive eruptions. J. Volcanol. Geotherm. Res. 255, 98–107.

CRAIG-APEI-SINTEGRA, 2013. http://www.craig.fr.

D'Oriano, C., Cioni, R., Bertagnini, A., Andronico, D., Cole, P., 2011. Dynamics of ash-dominated eruptions at Vesuvius: the post-512 AD AS1a event. Bull. Volcanol. 73, 699–715.

Daggitt, M., Mather, T., Pyle, D., Page, S., 2014. AshCalc—a new tool for the comparison of the exponential, power-law and Weibull model of tephra deposit. J. Appl. Volcanol. 3, 7.

Delcamp, A., van Wyk de Vries, B., Stéphane, P., Kervyn, M., 2014. Endogenous and exogenous growth of the monogenetic Lemptégy volcano, Chaîne des Puys, France. Geosphere 10 (5), 1–22.

Di Traglia, F., Cimarelli, C., de Rita, D., Gimeno Torrente, D., 2009. Changing eruptive style in basaltic explosive volcanism: examples from Croscat complex scoria cone, Garrotxa Volcanic Field (NE Iberian Peninsula). J. Volcanol. Geotherm. Res. 180, 89–109.

Erlund, E., Cashman, K., WWallace, P., Pioli, L., Rosi, M., Johnson, E., Delgado Granados, H., 2010. Compositional evolution of magma from Parícutin Volcano, Mexico: the tephra record. J. Volcanol. Geotherm. Res. 197, 167–187.

Eychenne, J., Le Pennec, J.L., Ramón, P., Yepes, H., 2013. Dynamics of explosive paroxysms at open-vent andesitic systems: high-resolution mass distribution analyses of the Tungurahua fall deposit (Ecuador). Earth Planet. Sci. Lett. 361, 343–355.

Fierstein, J., Nathenson, M., 1992. Another look at the calculation of fall tephra volumes. Bull. Volcanol. 54, 156–167.

Funiciello, R., Locardi, E., Lombardi, G., Parotto, M., 1976. The sedimentary ejecta from phreatomagmatic activity and their use for location of potential geothermal areas. Proceedings Geothermal Energy, International Congress on Thermal Waters, Geothermal Energy and Vulcanism of the Mediterranean Area. Athens, pp. 227–240.

Guilbaud, M.-N., Siebe, C., Agustín-Flores, J., 2009. Eruptive style of the young high-Mg basaltic andesitic Pelagatos scoria cone, southeast of México City. Bull. Volcanol. 71, 859–880.

Gurioli, L., Andronico, D., Bachelery, P., Balcone-Boissard, H., Battaglia, J., Boudon, G., Burgisser, A., Burton, M., Cashman, K., Cichy, S., Cioni, R., Di Muro, A., Dominguez, L., D'Oriano, C., Druitt, T., Harris, A.J.L., Hort, M., Kelfoun, K., Komorowski, J., Kueppers, U., Le Pennec, J.-L., Menand, T., Paris, R., Pioli, L., Pistolesi, M., Polacci, M., Pompilio, M., Ripepe, M., Roche, O., Rose-Koga, E., Rust, A., Schiavi, F., Scharff, L., Sulpizio, R., Taddeucci, J., Thordarson, T., 2015. MeMoVolc consensual document: a review of cross-disciplinary approach to characterizing small explosive magmatic eruptions. Bull. Volcanol. 77, 49.

Hardiagon, M., Troll, V., Annersten, B., van Wyk de Vries, B.D., Barker, A., Piquet, E., 2011. Explosive interaction between the crust and magma in the Beaunit tuff ring, Chaîne des Puys, France. Geophysical Research Abstracts. No. 13 in EGU2011-3465-1. EGU General Assembly 2011, Vienna.

Harris, A.J.L., Ripepe, M., 2007. Synergy of multiple geophysical approaches to unravel explosive eruption, conduit and source dynamics—a case study from stromboli. Chem. Erde 67, 1–35.

Heap, M., Xu, T., Chen, C., 2014. The influence of porosity and vesicle size on the brittle strength of volcanic rocks and magma. Bull. Volcanol. 76, 856.

Hintz, A., Valentine, G., 2012. Complex plumbing of monogenetic scoria cones: new insights from the Lunar Crater Volcanic Field (Nevada, USA). J. Volcanol. Geotherm. Res. 239-240, 19–32.

Houghton, B.F., Wilson, C.J.N., 1989. A vesicularity index for pyroclastic deposits. Bull. Volcanol. 51, 451–462.

Inman, D., 1952. Measures for describing the size distribution of sediments. J. Sediment. Petrol. 22 (3), 125–145.

Jannot, S., Schiano, P., Boivin, P., 2005. Melt inclusions in scoria and associated mantle xenoliths of Puy Beaunit Volcano, Chaîne des Puys, Massif Central, France. Contrib. Mineral. Petrol. 149, 600–612.

Johnson, E., Wallace, P., Cashman, K., Delgado Granados, H., Kent, A., 2008. Magma volatile contents and degassing-induced crystallization at Volcán Jorullo, Mexico: implications for melt evolution and the plumbing systems of monogenetic volcanoes. Earth Planet. Sci. Lett. 269, 478–487.

Johnson, P., Valentine, G., Cortés, J., Tadini, A., 2014. Basaltic tephra from monogenetic Marcath Volcano, central Nevada. J. Volcanol. Geotherm. Res. 281, 27–33.

Jordan, S.C., Cas, R.A.F., Hayman, P.C., 2013. The origin of a large (>3 km) maar volcano by coalescence of multiple shallow craters: Lake Purrumbete maar, southeastern Australia. J. Volcanol. Geotherm. Res. 254, 5–22.

Kawabata, E., Cronin, S., Bebbington, M., Moufi, M., El-Masry, N., Wang, T., 2015. Identifying multiple eruption phases from a compound tephra blanket: an example of the AD1256 Al-Madinah eruption, Saudi Arabia. Bull. Volcanol. 77, 6.

Kiyosugi, K., Horikawa, Y., Nagao, T., Itaya, T., Conner, C., Tanaka, K., 2014. Scoria cone formation through a violent Strombolian eruption: Irao Volcano, SW Japan. Bull. Volcanol. 76, 781.

Klawonn, M., Houghton, B., Swason, D., Fagents, S., Wessel, P., Wolfe, C., 2014. Constraining explosive volcanism: subjective choices during estimates of eruption magnitude. Bull. Volcanol. Geotherm. Res. 76, 793.

Mannen, K., Ito, T., 2007. Formation of scoria cone during explosive eruption at Izu-Oshima volcano, Japan. Geophys. Res. Lett. 34, L18302.

McGetchin, T., Settle, M., Chouet, B., 1974. Cinder cone growth model after Northeast Crater, Mount Etna, Sicily. J. Geophys. Res. 79 (23), 3257–3272.

Menand, T., Phillips, J., 2007. Gas segregation in dykes and sills. J. Volcanol. Geotherm. Res. 159, 393–408.

Menand, T., Tait, S., 2001. A phenomenological model for precursor volcanic eruptions. Nature 411, 678–680.

Miallier, D., Condomines, M., Pilleyre, T., Sanzelle, S., Guittet, J., 2004. Concordant thermoluminescence and $_{238}U - _{230}Th$ ages for a trachytic dome (Grand Sarcoui) from the Chaîne des Puys (French Massif Central). Quat. Sci. Rev. 23, 709–715.

Mitchell, K., 2005. Coupled conduit flow and shape in explosive volcanic eruptions. J. Volcanol. Geotherm. Res. 143, 187–203.

Németh, K., 2010. Monogenetic volcanic fields: origin, sedimentary record, and relationship with polygenetic volcanism. Geol. Soc. Am. Spec. Pap. 470, 43–66.

Palladino, D., Taddeucci, J., 1998. The basal ash deposit of the Sovana Eruption (Vulsini Volcanoes, central Italy): the product of a dilute pyroclastic density current. J. Volcanol. Geotherm. Res. 87, 233–254.

Parfitt, E.A., 2004. A discussion of the mechanisms of explosive basaltic eruptions. J. Volcanol. Geotherm. Res. 134, 77–107.

Pioli, L., Erlund, E., Johnson, E., Cashman, K., Wallace, P., Rosi, M., Delgado Granados, H., 2008. Explosive dynamics of violent Strombolian eruptions: the eruption of Parícutin Volcano 1943-1952 (Mexiko). Earth Planet. Sci. Lett. 271, 359–368.

Pioli, L., Azzopardi, B., Cashman, K., 2009. Controls on the explosivity of scoria cone eruptions: magma segregation at conduit junctions. J. Volcanol. Geotherm. Res. 186, 407–415.

Pyle, D.M., 1995. Assessment of the minimum volume of tephra fall deposits. J. Volcanol. Geotherm. Res. 69, 379–382.

Re, G., White, J., Ort, M., 2015. Dikes, sills, and stress-regime evolution during emplacement of the Jagged Rocks Complex, Hopi Buttes Volcanic Field, Navajo Nation, USA. J. Volcanol. Geotherm. Res. 295, 65–79.

Riedel, C., Ernst, G., Riley, M., 2003. Controls on the growth and geometry of pyroclastic constructs. J. Volcanol. Geotherm. Res. 127, 121–152.

Rowland, S., Jurado-Chichay, Z., Ernst, G., Walker, G., 2009. Pyroclastic deposits and lava flows from the 1759–1774 eruption of El Jorullo, Mexico: aspects of 'violent Strombolian' activity and comparison with Parícutin. In: Thordarson, T., Self, S., Larsen, G., Rowland, S., Hoskuldsson, A. (Eds.), Studies in Volcanology: The Legacy of George Walker. Vol. 2 of Special Publications of IAVCEI. Geological Society, London, pp. 105–128.

Ruth, D., Calder, E., 2014. Plate tephra: preserved bubble walls from large slug bursts during violent strombolian eruptions. Geology 42, 11–14.

Valentine, G., Krogh, K., 2006. Emplacement of shallow dikes and sills beneath a small basaltic volcanic centre—the role of pre-existing structure (Paiute Ridge, southern Nevada, USA). Earth Planet. Sci. Lett. 246, 217–230.

Valentine, G., Krier, D., Perry, F., Heiken, G., 2005. Scoria cone construction mechanisms, Lathrop Wells volcano, southern Nevada, USA. Geology 33 (8), 629–632.

Wohletz, K.H., 1983. Mechanics of hydrovolcanic pyroclast formation: grain-size, scanning microscopy, and experimental studies. J. Volcanol. Geotherm. Res. 17, 31–63.

Wood, C., 1980. Morphometric evolution of cinder cones. J. Volcanol. Geotherm. Res. 7, 387–413.

Zimanowski, B., Froehlich, G., Lorenz, V., 1991. Quantitative experiments on phreatomagmatic explosions. J. Volcanol. Geotherm. Res. 48, 341–358.